Environmental Science & Technology

Article

pubs.acs.org/est

Na^+, Ca^{2+}, and Mg^{2+} in Brines Affect Supercritical CO_2–Brine–Biotite Interactions: Ion Exchange, Biotite Dissolution, and Illite Precipitation

Yandi Hu, Jessica R. Ray, and Young-Shin Jun*

Department of Energy, Environmental and Chemical Engineering, Washington University in St. Louis, St. Louis, Missouri 63130, United States

Supporting Information

ABSTRACT: For sustainable geologic CO_2 sequestration (GCS), a better understanding of the effects of brine cation compositions on mica dissolution, surface morphological change, and secondary mineral precipitation under saline hydrothermal conditions is needed. Batch dissolution experiments were conducted with biotite under conditions relevant to GCS sites (55–95 °C and 102 atm CO_2). One molar NaCl, 0.4 M $MgCl_2$, or 0.4 M $CaCl_2$ solutions were used to mimic different brine compositions, and deionized water was used for comparison. Faster ion exchange reactions (Na^+–K^+, Mg^{2+}–K^+, and Ca^{2+}–K^+) occurred in these salt solutions than in water (H^+–K^+). The ion exchange reactions affected bump, bulge, and crack formation on the biotite basal plane, as well as the release of biotite framework ions. In these salt solutions, numerous illite fibers precipitated after reaction for only 3 h at 95 °C. Interestingly, in slow illite precipitation processes, oriented aggregation of hexagonal nanoparticles forming the fibrous illite was observed. These results provide new information for understanding $scCO_2$–brine–mica interactions in saline aquifers with different brine cation compositions, which can be useful for GCS as well as other subsurface projects.

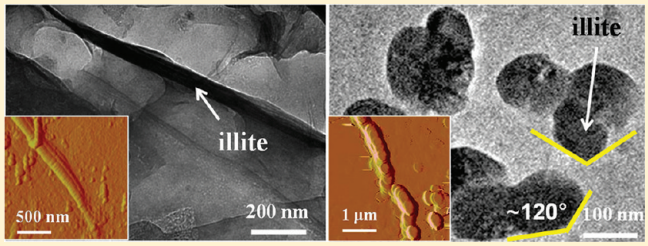

1. INTRODUCTION

Deep saline aquifers are one of the most promising options for geologic CO_2 sequestration (GCS) because of their large storage capacity.[1,2] For safe and efficient GCS operation, it is important to understand how CO_2 injection-induced mineral dissolution and precipitation affect the aquifer's porosity and permeability, which influence the caprock seal integrity and injectivity of CO_2.[3,4] For example, in the Tensleep saline aquifer in Wyoming, the permeability of five core samples decreased by around 16–44% after CO_2 injection.[5] Therefore, we need a better understanding of $scCO_2$–brine–mineral interactions and the effect of environmental factors on these interactions.

In different deep saline aquifers, the brine cation compositions vary greatly.[6−9] Based on field site investigations, sodium is the most abundant cation in most deep saline waters,[6−8] constituting 70% to >90% of total cations by mass.[6] Calcium is generally the second most abundant cation;[6,8] however, it could also be the most abundant cation in certain aquifers, and its concentration can be as high as 1.2 M.[6] In addition to Ca, there are also high concentrations of Mg.[6,8] For example, in Rose Sun sandstone, Ohio, the Mg concentration is 0.24 M.[7] The total electrolyte concentrations in brines can also vary greatly. For example, in the Michigan basin, Michigan, the salinity is over 400,000 mg/L, whereas at Silurian, Indiana, it is only 500 mg/L.[8] Hence, an improved understanding of cation effects on $scCO_2$–brine–mineral interactions is crucial.

Furthermore, maintaining caprock seal integrity is essential to prevent CO_2 leakage. Mica, a major component of caprock, is abundant at GCS sites.[9−11] The basal surface of micas usually carries a permanent negative charge,[12,13] where complexation, sorption, and ion-exchange reactions with the cations in brines could occur.[12] For different cations, their hydration states, water structures, and capacities for complexation, adsorption, and ion exchange reactions with the surfaces vary.[12,13] Therefore, specific cations can play different roles in $scCO_2$–brine–mica interactions.

In our previous study in 1 M NaCl solution at 95 °C and 102 atm CO_2,[14] fast Na^+–K^+ ion exchange occurred, causing the fast release of biotite framework ions and biotite surface cracking, which induced numerous fibrous illite precipitation and its detachment from the biotite surface. This is particularly important considering the short reaction times and potential impacts on permeability changes if numerous illite fibers form in a reservoir.[15] Different shapes of illite have been reported to differentially affect reservoir quality, such as permeability.[15] However, how the abundant cations in brines affect $scCO_2$–brine–mica interactions under GCS conditions is unknown.

The objective of this study was to investigate the effect of abundant Na^+, Mg^{2+}, and Ca^{2+} in brines on mica alteration (i.e.,

Special Issue: Carbon Sequestration

Received: March 31, 2012
Revised: May 2, 2012
Accepted: May 4, 2012

   dx.doi.org/10.1021/es301273g | Environ. Sci. Technol. XXXX, XXX, XXX–XXX

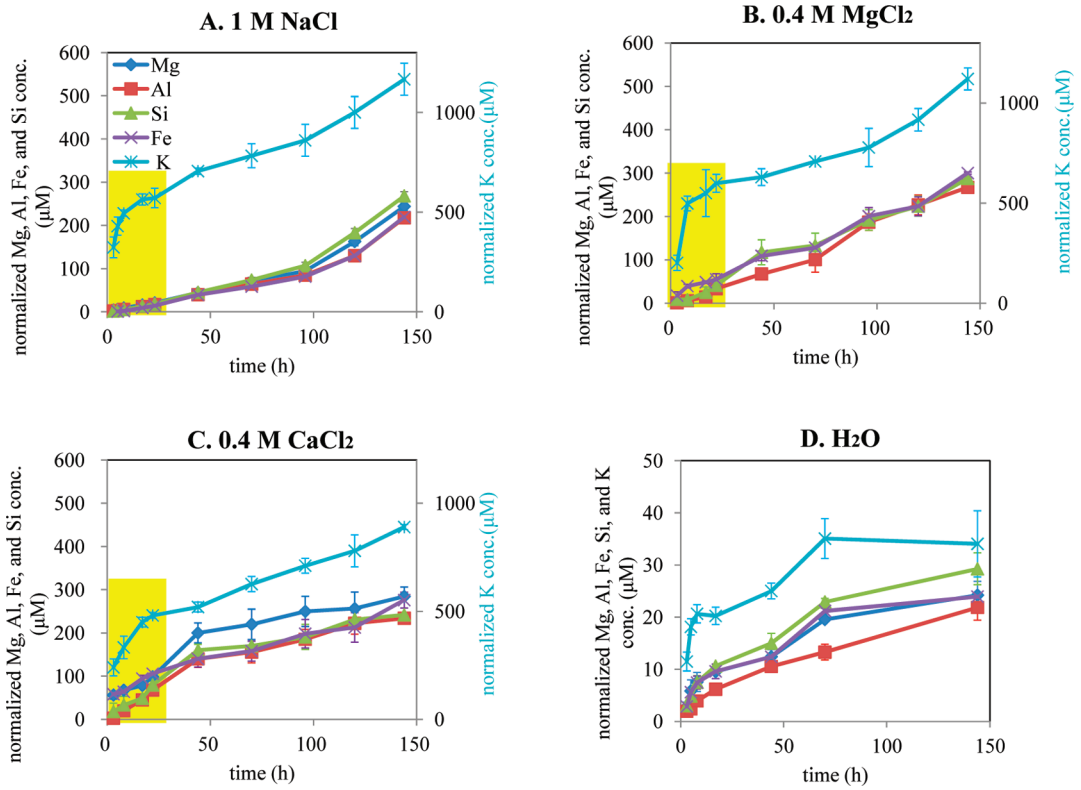

Figure 1. Dissolved ion concentrations from biotite after reaction in 1 M NaCl (A), 0.4 M $MgCl_2$ (B), 0.4 M $CaCl_2$ (C), and deionized water (D) for different times at 102 atm CO_2 and 95 °C. The concentrations are normalized by the stoichiometry of the biotite formula $[K_{0.91}Na_{0.08}(Mg_{0.52}Mn_{0.02}Fe_{0.37}Ti_{0.04})_3(Al_{1.00}Si_{3.00})O_{10}(F_{0.43}(OH)_{0.57})_2]$ to identify the dissolution congruency. For images A–C, the K concentrations are much higher than the framework ions (Mg, Fe, Al, and Si) and are read from the right *y*-axis.

dissolution, morphological evolution, and illite precipitation) under GCS conditions. Biotite was used as a model mica. Combining macroscopic fluid chemistry and microscopic surface analysis techniques, this study provides unique information on $scCO_2$–brine–mica interactions under GCS conditions.

2. EXPERIMENTAL SECTION

2.1. Chemicals and Minerals. All chemicals used were at least ACS grade. Ultrapure water (18.2 mΩ·cm at 25 °C) was used to prepare the salt solutions (1 M NaCl, 0.4 M $MgCl_2$, and 0.4 M $CaCl_2$ solutions). In previous studies, significant effects of salinity on mica alteration have been reported;[9,14,16,17] thus, the salt concentrations were chosen to have the same salinity and also to be relevant to GCS sites.[6−8]

Biotite samples were obtained from Ward's Natural Science, NY. The elemental compositions $[K_{0.91}Na_{0.08}(Mg_{0.52}Mn_{0.02}Fe_{0.37}Ti_{0.04})_3(Al_{1.00}Si_{3.00})O_{10}(F_{0.43}(OH)_{0.57})_2]$ characterized with both electron microprobe (EMP) and X-ray fluorescence (XRF) were in good agreement. Biotite crystals were cleaved to thin samples (~100 ± 20 μm) along the {001} cleavage surface (basal plane), cut into 2.5 cm × 0.8 cm flakes, and cleaned.

2.2. High Pressure/Temperature Experiments, Analytical Methods, and Thermodynamic Calculations. A biotite flake and 4 mL of salt solution or deionized water (for comparison) were put in a PTFE tube inside the reactor (Parr Instrument Company, IL). Then the reactor was sealed and pressurized CO_2 was injected. Batch experiments were conducted at 102 atm CO_2 and 95 °C for elapsed times of 3, 8, 17, 22, 44, 70, 96, 120, and 144 h. The pressure and temperature were chosen based on reported parameters for GCS sites,[18] and they allowed obtaining experimental results within a reasonable time. A few experiments were conducted at lower temperatures (55, and 65 °C) in 1 M NaCl solution, to investigate the effect of illite precipitation kinetics on its shape. To compare with the situation without CO_2 injection, a 6 day batch experiment was also conducted at 102 atm N_2 and 95 °C in 1 M NaCl solution.

After reaction, the dissolved ion concentrations in solution were measured by inductively coupled plasma-mass spectrometry (ICP-MS, 7500ce, Agilent Technologies, CA). The reacted biotite basal surfaces were observed with atomic force microscopy (AFM, Nanoscope V Multimode SPM, Veeco). Both contact and tapping mode AFM were used. Contact mode was used to scan larger surface areas, while tapping mode was used to scan smaller surface areas for recording more detailed morphology. To identify the mineral phase of the precipitates, the reacted biotite samples were sonicated for 30 min to detach the precipitates from the surface, and a drop of this suspension was placed on a Formvar/carbon-coated Cu grid. The electron diffraction patterns of the precipitates were measured using high resolution-transmission electron microscopy (HR-TEM, JEOL JEM-2100F field emission), to determine the atomic *d*-spacings of the precipitates.

Using Duan and Sun (2003)'s equations,[19] we calculated the dissolved CO_2 concentrations at 102 atm and 95 °C in different solutions. Using the dissolved CO_2 concentrations and the dissolved ion concentrations measured by ICP-MS, the cation activities and the pH values throughout the experiments were calculated using Geochemists' Workbench (GWB, Release 8.0, RockWare, Inc.). Details of the sample preparation, exper-

dx.doi.org/10.1021/es301273g | Environ. Sci. Technol. XXXX, XXX, XXX−XXX

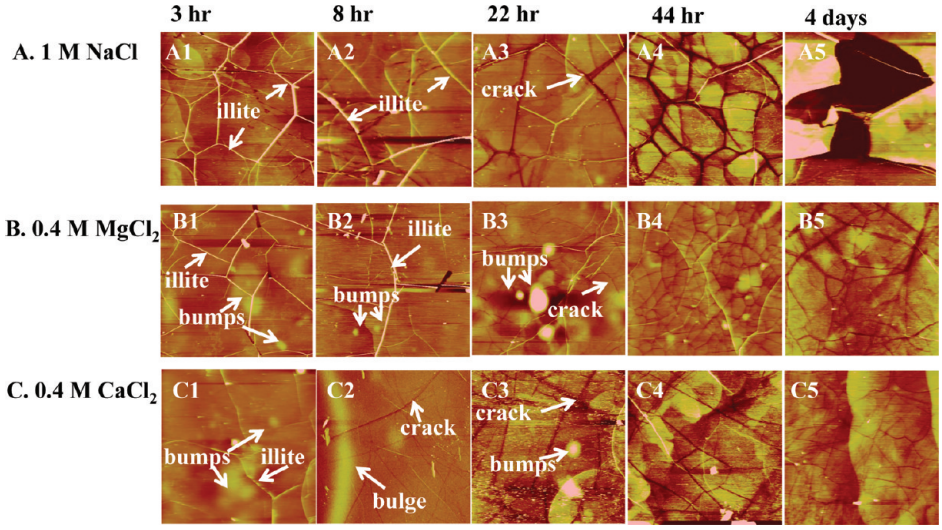

Figure 2. Contact mode AFM observations of the biotite basal planes after reaction in 1 M NaCl (A), 0.4 M $MgCl_2$ (B), and 0.4 M $CaCl_2$ (C) at different elapsed reaction times at 102 atm CO_2 and 95 °C. The AFM image size is 50 × 50 μm, and the height scale is 50 nm.

imental setup, AFM operation, and thermodynamic calculations are given in the Supporting Information (SI).

3. RESULTS AND DISCUSSION

3.1. Ion Exchange Reactions and K^+ Release from Biotite. Preferential release of the biotite interlayer K^+ over the framework ions (Mg, Fe, Al, and Si) was observed in all solutions (Figures 1A–D), occurring through ion exchange reactions (Na^+–K^+, Mg^{2+}–K^+, Ca^{2+}–K^+, and H^+–K^+). Throughout the 6 day experiments, the released K concentrations in the salt solutions were 24 ± 5 times higher than in water (Figures 1A–D). Among the salt solutions, the released K concentrations were similar in the NaCl and $MgCl_2$ solutions, and slightly higher than in the $CaCl_2$ solution (Figures 1A–C).

The released K concentrations in these solutions can result from the ion exchange rates. Therefore, several mechanisms were considered as controlling the ion exchange rates. First, higher cation activities in the bulk solution can accelerate the ion exchange reactions,[20] and cation activities in the bulk solution can be affected by both their activity coefficients and complexation with anions. Calculated with GWB (SI Table S2), the H^+, Na^+, Mg^{2+}, and Ca^{2+} activities were 0.0005, 0.60, 0.08, and 0.05 M in water, 1 M NaCl, 0.4 M $MgCl_2$, and 0.4 M $CaCl_2$ solutions, respectively. Based on these calculations, in water, the H^+ activity (0.0005 M) was 2–3 orders of magnitude lower than the activities of other cations, which explained the much slower exchange in water (H^+–K^+) than in the salt solutions (Na^+–K^+, Mg^{2+}–K^+, and Ca^{2+}–K^+). Among the salt solutions, Mg^{2+} (0.08 M) and Ca^{2+} (0.05 M) activities were around 1 order of magnitude lower than that of Na^+ (0.60 M). Considering the cation activity effect on the ion exchange rate, the Mg^{2+}–K^+ and Ca^{2+}–K^+ ion exchange should be much slower than the Na^+–K^+ ion exchange. However, the released K concentrations in these salt solutions were similar, thus, there must be other mechanisms affecting the ion exchange reactions.

Second, H^+ can facilitate cation exchange with mica interlayer K^+.[21] However, GWB calculations (SI Table S2) showed that the pH values in different salt solutions were similar (the difference in pH values was within 0.34 throughout the 6 days experiment). Thus, the pH effect on ion exchange among these solutions is minor.

Third, the cation exchange reactions in these salt solutions were fast, and their rates were transport controlled instead of the surface reaction controlled.[22] Thus, the local cation concentrations near the biotite surface should also be considered. Mica minerals carry negative charges, and thus attract cations to their surfaces.[13] These adsorbed cations result in higher local cation concentrations near the surface than in the bulk.[13] Different rates and orders of adsorption are known among the cations, depending on the surface potential, valence, and hydrodynamic radius.[13] The order of cation preference by soil surfaces is known as the Lyotropic Series, where preferential adsorption of Mg^{2+} and Ca^{2+} over Na^+ to mineral surfaces has been broadly reported, although the preference order between Mg^{2+} and Ca^{2+} varied among these reports.[13,20,22] Therefore, more local Mg^{2+} and Ca^{2+} than Na^+ are available to exchange with K^+.

Based on the reasoning above, we summarized that Mg^{2+} and Ca^{2+} have lower activities in bulk solution; however, their higher surface preference over Na^+ can cause high local Mg^{2+} and Ca^{2+} concentrations near the biotite surface. Therefore, the opposing impacts can be offset causing the net aqueous K^+ concentrations in all salt solutions to be similar.

3.2. Morphological Evolutions of Biotite Basal Surfaces and Relevance to Ion Exchange Reactions. Contact mode AFM analysis (Figure 2 and SI Figure S2) shows that the morphological changes of biotite basal surfaces after reaction are greatly influenced by different cations in brines. After reaction in the salt solutions for only 3 h, bumps and dendritic bulges formed on the biotite basal surfaces. Their abundance followed the order: $CaCl_2$ > $MgCl_2$ > NaCl (Figures 2A1, 2B1, and 2C1). After reaction for 8 h, cracks were first observed after reaction in $CaCl_2$ (Figure 2C2). AFM observations have been conducted on mica basal surfaces after reaction in NaCl solution, and bump, bulge, and crack formation have been observed, which resulted from the swelling of the mica basal surface caused by Na^+–K^+ ion exchange.[9,14,23] The similar morphologies of bump, bulge, and crack formation on mica after reaction in $CaCl_2$ and $MgCl_2$ solutions observed

dx.doi.org/10.1021/es301273g | Environ. Sci. Technol. XXXX, XXX, XXX–XXX

here were also thought to be caused by cation exchange reactions.

Different swelling levels of mica caused by cation exchange have been previously reported by *d*-spacing measurement. With K^+, Na^+, Mg^{2+}, and Ca^{2+} as the interlayer cation, the *d*-spacings of phlogopite (magnesium mica) were reported to be 10.1, 12.3, 14.6, and 14.8 Å, respectively, and the H_2O contents in the samples as a weight percentage were < 0.1%, 10.2%, 10.6%, and 11.9%, respectively.[24] The order of swelling for cation exchange reactions agreed with the hydrated cation sizes: Ca^{2+} > Mg^{2+} > Na^+.[25,26] Among the salt solutions, the released K concentrations were similar (Figure 1), while cracking occurred fastest after reaction with $CaCl_2$ solution, and fewest bumps formed after reaction with NaCl solution. Based on our observations of the swelling-induced morphology (bumps, bulges, and cracks) and the reported swelling effects[24] and hydrated cation sizes,[25,26] we suggest that when larger hydrated cations get into the biotite interlayer through ion exchange, more significant expansion of the biotite layer occurs, which could promote bump, bulge, and crack formation.

After reaction for 22 h, the biotite basal surfaces cracked in all these salt solutions (Figures 2A3, 2B3, and 2C3). Interestingly, as the reactions continued (44−144 h), after reaction with $CaCl_2$ (Figures 2C4−5) and $MgCl_2$ (Figures 2B4−5) solutions, numerous smaller cracks formed, with depths similar to the earlier ones (∼10−20 nm throughout the 22−144 h reactions); while after reacting with NaCl solution, the depth of the cracks grew from 13.4 ± 5.0 to 57.5 ± 7.6 nm throughout the 22−70 h reaction (the surface after reaction for 44 h is shown in Figure 2A4). Disintegration of the biotite basal plane (Figure 2A5) and release of the surface layer into solution also occurred. The mechanisms of different crack evolutions in the solutions are not clear at this moment, and are not the focus of this study.

In contrast, in water, the occurrence of bumps was rare, and neither bulges nor cracks were observed throughout the reaction period (SI Figure S3). These differences can stem from the following reasons: First, the H^+−K^+ ion exchange was much slower than the ion exchange reactions in the salt solutions, as discussed in Section 3.1. Second, the hydrated H^+ was much smaller than all the hydrated metal cations (Na^+, Mg^{2+}, and Ca^{2+}), indicating that H^+−K^+ ion exchange causes much less swelling of the biotite layer than the ion exchange reactions in the salt solutions. Both mechanisms hindered bump, bulge, and crack formation in water.

3.3. Release of Biotite Framework Ions and Its Relevance to Ion Exchange Reactions and Morphological Changes. Throughout the experiments in water, the dissolved framework ion concentrations from biotite (Mg, Al, Si, and Fe) were around 1 order of magnitude lower than those in the salt solutions (Figure 1). In the salt solutions, faster ion exchange, more significant swelling, and more pronounced morphological changes were thought to have promoted the release of the framework ions.

Among the salt solutions, at the early stage of reaction (the shaded region in Figure 1), the dissolved framework ion concentrations followed the order: $CaCl_2$ > $MgCl_2$ > NaCl. Considering that this order agreed with that of the expansion caused by the different ion exchange reactions,[24] and the pH and ionic strength values of the salt solutions were similar (SI Table S2), we suggest that the release rates of the framework ions were controlled by the expansion caused by the ion exchange reactions. The bigger the hydrated cation, the more significant the expansion and stress build up, which could weaken the bonds between the biotite framework ions with oxygen, promoting their release. In addition, in the $CaCl_2$ solution, the early crack formation after reaction for only 8 h (Figure 2C2) created more edge surface area of biotite in contact with solution, which further promoted the dissolution (Figure 1C). In the later stage, after reaction for 22 h in both 1 M NaCl and 0.4 M $MgCl_2$ solutions, the release rates accelerated (Figures 1A and 1B). The increased release rates were linked with the new edge surface areas generated through crack formation; After reaction for 96 h in 1 M NaCl solution, as discussed in our previous work,[14] the disintegration and detachment of the biotite surface layer further increased the biotite surface area in contact with solution, and thus further increased the framework ion release rates (Figure 1A).

3.4. Fibrous Illite Precipitation and Its Detachment from the Surface. In our previous study,[14] numerous illite fibers formed on the biotite surface after reaction in 1 M NaCl for only 3 h. In the current study, numerous fibrous precipitates were also observed on the biotite surface after reaction for 3 h in all three salt solutions (Figures 2A1, B1, and C1). They were confirmed to be illite, based on their fibrous shape, the characteristic 120°, and their diffraction patterns measured by HR-TEM (Figures 3A−C). However, in water, no macroscopic fibrous illite was observed throughout the experiments (SI Figure S3).

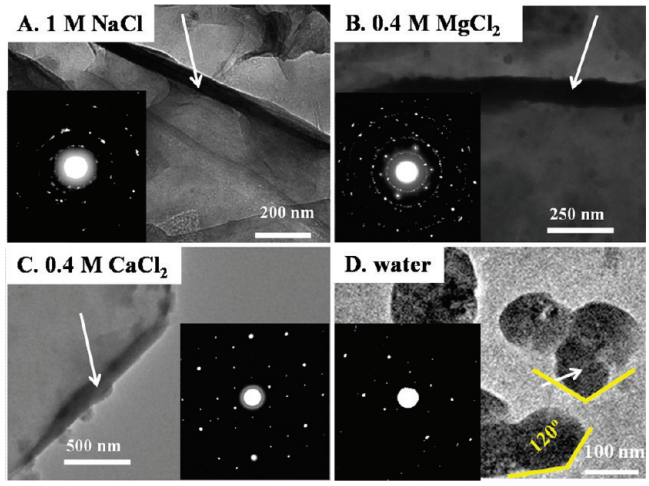

Figure 3. HRTEM results for secondary mineral phase identification after reaction of biotite in 1 M NaCl (A), 0.4 M $MgCl_2$ (B), 0.4 M $CaCl_2$ (C), and deionized water (D) at 102 atm CO_2 and 95 °C. The insets are the electron diffraction patterns collected from the areas indicated by the arrows.

To observe the details of the precipitates on the biotite surfaces, tapping mode AFM images were obtained. After reaction in 1 M NaCl at 95 °C for 3 h (Figure 4A), the ends of the illite fibers (their growth directions) were observed as the oriented aggregates of nanoparticles. After reaction in DI water, hexagonal nanoparticles were observed on the biotite surface. Most of the nanoparticles were randomly distributed, but a few started to accumulate in a line, showing an overall fibrous shape (Figure 4B). Interestingly, the hexagonal nanoparticles after reaction in water were also confirmed to be illite, based on their electron diffraction patterns measured by HRTEM (Figure 3D). To the best of our knowledge, this is the first time that direct nanoscale observations were made of the oriented

dx.doi.org/10.1021/es301273g | *Environ. Sci. Technol.* XXXX, XXX, XXX−XXX

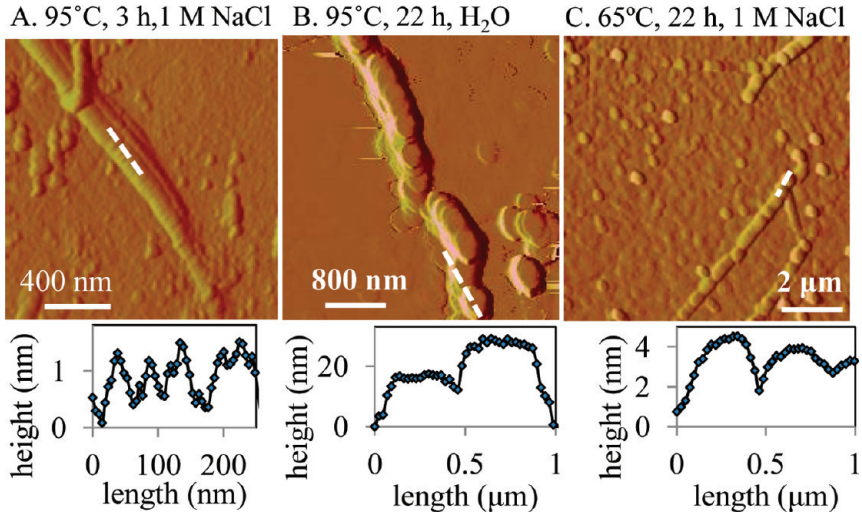

Figure 4. Tapping mode AFM observations of the biotite basal surface after reaction at 102 atm CO_2. The temperatures and solution compositions are shown in the figures. These amplitude mode images clearly show the morphology of the hexagonal nanoparticles. The height profiles below the AFM images are cut along the dashed lines in the corresponding AFM height mode images.

aggregation of small hexagonal nanoparticles forming fibrous illite.

Both elongated- (such as fibrous) and platy- (such as hexagonal) shaped illite has been reported in both field site observations and laboratory illite synthesis (SI Table S1 and Figure S5). Fibrous-shaped illite can lower the permeability in porous media much more significantly than the platy−shaped illite.[15] Thus, a significant amount of research has been performed to study the mechanisms for the fibrous illite formation; however, there is no definite answer to this question yet. In recent decades, oriented aggregation has been widely observed for nanoparticle growth, such as TiO_2 and iron oxides nanoparticles.[27,28] It was thought to be a nonclassical growth mechanism that differed from Ostwald ripening.[29,30] Based on our observations, we suggest that where slower illite formation kinetics occur, individual hexagonal nanoparticles form and oriented aggregation occurs to form the fibrous shape. When faster illite formation kinetics occur, the illite quickly forms aggregations of small particles and grows as fibrous shapes. In water, the dissolved ion concentrations, especially K, were significantly lower than those in the salt solutions. Thus, much less illite formed, and during the slow illite precipitation, individual hexagonal particles precipitated, and some assembled as oriented aggregates to form the fibrous shape (Figure 4B). In the salt solutions, the fast ion release resulted in numerous illite precipitation; also, during this fast precipitation, the small illite particles aggregated fast and grew as fibrous shapes (Figure 4A). This hypothesis was further confirmed by AFM observations of the biotite surface after reaction in 1 M NaCl solution at 65 °C. At this lower temperature, the dissolution and illite precipitation were slower than at 95 °C, and the oriented aggregation of small hexagonal precipitates forming the fibrous shape was also observed (Figure 4C).

Throughout the experiments, bumps, bulges, and cracks on biotite surfaces were observed to control the amount of illite fibers on the biotite surface (Figure 2). During the early stage (3−17 h), their abundance on the biotite surface after reaction in the salt solutions followed the order: NaCl > $MgCl_2$ > $CaCl_2$, which is opposite to the trend of the abundance of bump, bulge, and crack formation (Figures 2A1−2, 2B1−2, and 2C1−2). In the later stage (22−144 h), when cracking of biotite surfaces occurred in all the salt solutions, the amount of fibrous illite on all the biotite surfaces diminished (Figures 2A3−5, 2B3−5, and 2C3−5). It is possible that when illite precipitated on the biotite surface, epitaxial interaction between illite and the biotite substrate occurred. Thus, when bumps, bulges, and cracks formed on the biotite surface, stress could build up in the bonds between the fibrous illite and the deformed biotite substrate, resulting in the easy detachment of fibrous illite and the inhibition of the epitaxial illite formation on mica. The exact mechanism governing this phenomenon requires further investigation.

3.5. Enhanced Biotite Dissolution and Morphological Evolution by CO_2 Injection. Experiments conducted in 1 M NaCl for 6 days under 102 atm CO_2/N_2 were compared. The released biotite interlayer K concentration after reaction under N_2 for 6 days was only 60% of that under CO_2 (SI Table S4). With CO_2 injection, the dissolved proton concentration was significantly higher, thus, the synergetic effect of protons on the cation exchange promoted the K release.[21] For the biotite framework ions, the released concentrations were more than 40 times higher after reaction under CO_2 than under N_2, indicating CO_2 injection at GCS sites will cause significantly enhanced mica dissolution.

In the experiment conducted in 1 M NaCl under N_2 gas for 6 days, bumps and fibrous illite were observed on the biotite surface, but no cracks appeared (SI Figure S6) although the dissolved K concentration was 25% higher than those after reaction in 1 M NaCl under CO_2 for 22 h when cracks were already observed. Thus, the cracking formation is not related solely to cation exchange and K release. It could also be related to the release of biotite framework ions, or the presence of $scCO_2$, which might enhance crack formation.

4. ENVIRONMENTAL IMPLICATIONS

In this study, using multidisciplinary techniques providing macroscopic aqueous chemistry and microscopic surface morphology analysis, we show that brine cation composition can control the ion exchange reactions with biotite interlayer K, as well as the resulting surface morphological evolutions and biotite framework ion release (Mg, Al, Fe, and Si). We observed that the relative abundance of morphologies caused by swelling

dx.doi.org/10.1021/es301273g | Environ. Sci. Technol. XXXX, XXX, XXX−XXX

(such as bumps, bulges, and cracks) and that the early stage release rate of biotite framework ions followed the same order: $CaCl_2$ > $MgCl_2$ > NaCl ≫ water, which agreed with the order of the hydrated cation size[25,26] and the expansion caused by the different ion exchange reactions.[24] Thus, we suggest that the larger hydrated cations can cause more stress on the biotite structure through ion exchange reaction, which can promote bump, bulge, and crack formation, as well as the release of the biotite framework ions.

Brine cation composition also affects the kinetics of illite precipitation as well as the resulting shape. During slow illite precipitation, the oriented aggregates of hexagonal nanoparticles forming the fibrous illite were directly observed for the first time. This observation suggests new possible mechanisms for fibrous illite formation. Precipitation of fibrous illite in sandstone pores has attracted much interest because the illite fibers can lower the permeability in porous media significantly and cause serious problems for hydrocarbon production.[15] Our observations provide insight for future work to improve the understanding of the fundamental mechanisms controlling the morphology of illite precipitates.

■ ASSOCIATED CONTENT

Supporting Information

Descriptions of the experimental details, six figures (experimental setup, illite crystal planes and shapes, and more AFM images) and four tables are available free of charge via the Internet at http://pubs.acs.org.

■ AUTHOR INFORMATION

Corresponding Author

*Phone: (314) 935-4539; fax: (314) 935-7211; e-mail: ysjun@seas.wustl.edu; http://encl.engineering.wustl.edu/.

Notes

The authors declare no competing financial interest.

■ ACKNOWLEDGMENTS

This work is supported by the NSF CAREER AWARD (EAR-1057117), and Y. Hu was partially supported by the Director, Office of Science, the Office of Basic Energy Sciences of the U.S. Department of Energy, in association with the Energy Research Frontier Center of Berkeley Lab, under Contract No. DE-AC02-05CH11231. We would like to acknowledge Dr. Ian Bourg for valuable discussion.

■ REFERENCES

(1) Bachu, S. Sequestration of CO_2 in geological media: criteria and approach for site selection in response to climate change. *Energy Convers. Manage* **2000**, *41* (9), 953−970.

(2) Metz, B.; Davidson, O.; Coninck, H. D.; Loos, M.; Meyer, L. *Special Report on Carbon Dioxide Capture and Storage*; IPCC: Cambridge, England, 2005.

(3) White, C. M.; Strazisar, B. R.; Granite, E. J.; Hoffman, J. S.; Pennline, H. W. Separation and capture of CO_2 from large stationary sources and sequestration in geological formations-coalbeds and deep saline aquifers. *J. Air Waste Manage. Assoc.* **2003**, *53*, 645−715.

(4) Luquot, L.; Gouze, P. Experimental determination of porosity and permeability changes induced by injection of CO_2 into carbonate rocks. *Chem. Geol.* **2009**, *265* (1−2), 148−159.

(5) Shiraki, R.; Dunn, T. L. Experimental study on water-rock interactions during CO_2 flooding in the Tensleep Formation, Wyoming, USA. *Appl. Geochem.* **2000**, *15* (3), 265−279.

(6) Kharaka, Y. K.; Hanor, J. S., Deep fluids in the continents: I. sedimentary basins. In *Treatise on Geochemistry*; Drever, J. I., Ed.; Elsevier: Oxford, 2007; Vol. *5*, pp 1−48.

(7) Breen, K. J.; Angelo, C. G.; Masters, R. W.; Sedam, A. C. *U.S. Geological Survey: Water Resources Investigation Report (84-4314)*; Ohio Department of Natural Resources, Division of Oil and Gas: Columbus, OH, 1985.

(8) Keller, S. J. *Analyses of Subsurface Brines of Indiana*; Department of Natural Resources: Bloomington, 1983.

(9) Shao, H.; Ray, J. R.; Jun, Y.-S. Effects of salinity and the extent of water on supercritical CO_2-induced phlogopite dissolution and secondary mineral formation. *Environ. Sci. Technol.* **2011**, *45* (4), 1737−1743.

(10) Shao, H.; Ray, J. R.; Jun, Y.-S. Dissolution and precipitation of clay minerals under geologic CO_2 sequestration conditions: CO_2−brine−phlogopite interactions. *Environ. Sci. Technol.* **2010**, *44* (15), 5999−6005.

(11) Cole, D. R.; Chialvo, A. A.; Rother, G.; Vlcek, L.; Cummings, P. T. Supercritical fluid behavior at nanoscale interfaces: Implications for CO_2 sequestration in geologic formations. *Philos. Mag.* **2010**, *90*, 2339−2363.

(12) Schlegel, M. L.; Nagy, K. L.; Fenter, P.; Cheng, L.; Sturchio, N. C.; Jacobsen, S. D. Cation sorption on the muscovite (001) surface in chloride solutions using high-resolution X-ray reflectivity. *Geochim. Cosmochim. Acta* **2006**, *70* (14), 3549−3565.

(13) Tan, K. H., *Principles of Soil Chemistry*; CRC Press, Taylor & Francis Group: Boca Raton, 2010.

(14) Hu, Y. D.; Ray, J. R.; Jun, Y. S. Biotite-brine Interactions under acidic hydrothermal conditions: fibrous illite, goethite, and kaolinite formation and biotite surface cracking. *Environ. Sci. Technol.* **2011**, *45* (14), 6175−6180.

(15) Lander, R. H.; Bonnell, L. M. A model for fibrous illite nucleation and growth in sandstones. *AAPG Bull.* **2010**, *94* (8), 1161−1187.

(16) Garcia, D.; Shao, H.; Hu, Y.; Ray, J. R.; Jun, Y.-S. Supercritical CO_2-brine induced dissolution, swelling, and secondary mineral formation on phlogopite surfaces at 75−95°C and 75 atm. *Energy Environ. Sci.* **2012**, *5*, 5758−5767.

(17) Yang, Y.; Ronzio, C.; Jun, Y.-S. The effects of initial acetate on $scCO_2$-brine-anorthite interactions under geologic CO_2 sequestration conditions. *Energy Environ. Sci.* **2011**, *4*, 4596−4606.

(18) Xu, T.; Kharaka, Y. K.; Doughty, C.; Freifeld, B. M.; Daley, T. M. Reactive transport modeling to study changes in water chemistry induced by CO_2 injection at the Frio-I Brine Pilot. *Chem. Geol.* **2010**, *271*, 153−164.

(19) Duan, Z. H.; Sun, R. An improved model calculating CO_2 solubility in pure water and aqueous NaCl solutions from 273 to 533 K and from 0 to 2000 bar. *Chem. Geol.* **2003**, *193* (3−4), 257−271.

(20) McDonald, L. M.; Evangelou, V. P.; Chappell, M. A., Cation exchange. In *Encyclopedia of Soils in the Environment*; Hillel, D., Ed.; Elsevier Academic Press: Oxford, 2005; Vol. *1*, p 183.

(21) Newman, A. C. D. The synergetic effect of hydrogen ions on the cations exchange of potassium in micas. *Clay Miner.* **1970**, *8*, 361−373.

(22) Sposito, G., *the Chemistry of Soils*; Oxford University Press: New York, 2008.

(23) Sanchez-Pastor, N.; Aldushin, K.; Jordan, G.; Schmahl, W. W. K^+-Na^+ exchange in phlogopite on the scale of a single layer. *Geochim. Cosmochim. Acta* **2010**, *74* (7), 1954−1962.

(24) Bortun, A. I.; Bortun, L. N.; Khainakov, S. A.; Clearfield, A. Ion exchange properties of the sodium phlogopite and biotite. *Solvent Extr. Ion Exch.* **1998**, *16* (4), 1067−1090.

(25) Ikeda, T. Hydration properties of magnesium and calcium ions from constrained first principles molecular dynamics. *J. Chem. Phys.* **2007**, *127*, 074503.

(26) Ikeda, T. Hydration of alkali ions from first principles molecular dynamics revisited. *J. Chem. Phys.* **2007**, *126*, 034501.

(27) Tsai, M. H.; Chen, S. Y.; Shen, P. Imperfect oriented attachment: Accretion and defect generation of nanosize rutile condensates. *Nano Lett.* **2004**, *4* (7), 1197−1201.

(28) Guyodo, Y.; Mostrom, A.; Penn, R. L.; Banerjee, S. K., From Nanodots to Nanorods: Oriented aggregation and magnetic evolution of nanocrystalline goethite. *Geophys. Res. Lett.* **2003**, *30*, (10).
(29) Penn, R. L.; Banfield, J. F. Imperfect oriented attachment: Dislocation generation in defect-free nanocrystals. *Science* **1998**, *281* (5379), 969−971.
(30) Penn, R. L.; Tanaka, K.; Erbs, J. Size dependent kinetics of oriented aggregation. *J. Cryst. Growth* **2007**, *309* (1), 97−102.